



LAWRENCE
LIVERMORE
NATIONAL
LABORATORY

Probing of the hydrogen melting line at high pressures by dynamic compression

A. Grinenko, D.O. Gericke, S. H. Glenzer, J. Vorberger

June 19, 2008

Physical Review Letters

Disclaimer

This document was prepared as an account of work sponsored by an agency of the United States government. Neither the United States government nor Lawrence Livermore National Security, LLC, nor any of their employees makes any warranty, expressed or implied, or assumes any legal liability or responsibility for the accuracy, completeness, or usefulness of any information, apparatus, product, or process disclosed, or represents that its use would not infringe privately owned rights. Reference herein to any specific commercial product, process, or service by trade name, trademark, manufacturer, or otherwise does not necessarily constitute or imply its endorsement, recommendation, or favoring by the United States government or Lawrence Livermore National Security, LLC. The views and opinions of authors expressed herein do not necessarily state or reflect those of the United States government or Lawrence Livermore National Security, LLC, and shall not be used for advertising or product endorsement purposes.

Probing of the hydrogen melting line at high pressures by dynamic compression

A. Grinenko¹, D.O. Gericke¹, S.H. Glenzer², and J. Vorberger¹

¹*Centre for Fusion, Space and Astrophysics, Department of Physics,
University of Warwick, Coventry CV4 7AL, United Kingdom*

²*L-399, Lawrence Livermore National Laboratory, P.O. Box 808, Livermore, CA 94551, USA*

(Dated: June 6, 2008)

We investigate the capabilities of dynamic compression by intense heavy ion beams to yield information about the high pressure phases of hydrogen. Employing *ab initio* simulations and experimental data, a new wide range equation of state for hydrogen that covers solid, fluid, gas and plasma phases has been constructed for our hydrodynamic simulations. The results show that the melting line up to its maximum as well as the transition from the molecular fluid to the fully ionized, metallic phase can be tested with the beam parameters available at the upcoming FAIR facility at GSI-Darmstadt. Using the structural information from the *ab initio* simulations, we also demonstrate that x-ray scattering is capable of extracting the information about the structure and the dissociation state.

PACS numbers: 52.27.Gr, 51.30.+i, 41.75.Ak

Experimental and theoretical investigations concerning the thermodynamic and structural properties of hydrogen continue to break new ground. Despite its seemingly simple composition, hydrogen is known to have a variety of complex phases [1]. Moreover, both experimental [2–9] and theoretical [10–14] methods have so far failed to give conclusive answers concerning the existence of a plasma phase transition, the nature of the molecular to atomic transition in the high density fluid, the location of the metallization transition in the solid, the melting line for pressures higher than 250 GPa [15] and the question of a possible liquid at $T = 0$ K connected to it [16].

Answers to these basic questions are required urgently as new discoveries in astrophysics and the developments for inertial confinement fusion continue to demand more accurate equation of state (EOS) data. Biased by detection methods, most extrasolar planets discovered are giant gas planets [17–19]. Even Jupiter and Saturn, although much better understood, still hold secrets about their inner structure [20] that can only be revealed by combining very precise EOS data and planet modelling [21]. Similar demands on the EOS are made by simulations of inertial fusion capsules, including fast ignition [22–24]. Since the targets are heated and compressed from a cryogenic state, the intermediate states to the burning fusion plasma are highly correlated solids or fluids and the compression path crosses a number of known and proposed phase transitions.

Although several well-established techniques to create high pressure samples exist, e.g., static compression in diamond anvil cells [1] and shocks driven by high-power lasers [6] or high explosives [9], the accessible parameter space is rather limited. Dynamic compression driven by intense heavy ion beams is an alternative approach that can considerably extend this space. Here, we focus on the capabilities of a proposed design that deposits the beam energy into a hollow cylinder (absorber) which in turn compresses the hydrogen embedded in the center

[25–27]. By carefully tuning the beam parameters, we show that such an experiment is able to reach molecular solid and fluid states, metallic fluids, and the region around the maximum of the melting line including parts where the melting line of hydrogen is predicted to have a negative slope [15]. Thus, our understanding of two basic phase transitions, high pressure melting and pressure ionization, can be tested. The beam parameters needed are well within reach of the FAIR facility being built at the Gesellschaft für Schwerionenforschung (GSI) in Darmstadt, Germany.

We perform hydrodynamic simulations to investigate the hydrogen states accessible by ion beam driven compression using our Lagrangian-Eulerian remap code. The numerical scheme is explicit, in second order accurate, and uses the standard arbitrary viscosity term for shock smoothing [28]. The remap step allows to control the grid at every time step using the second order Van Leer advection algorithm [29]. It is purely geometric; the physics is fully included in the Lagrangian step. The code allows for remapping to any arbitrary constant or moving grid that satisfies the stability conditions. In our simulations the absorber-hydrogen boundary was constantly tracked and a new smoothed grid was calculated at every time step such that each grid cell contains one material only.

The beam parameters and target dimensions used here are similar to those in Ref. [27]. The target consists of the absorber made of lead or aluminum in the form of a hollow cylinder with an inner radius of 0.4 mm, an outer radius of 3.0 mm and length of 1 cm. This shell is filled with cryogenic hydrogen initially at a temperature of $T = 14$ K and a density of $\rho = 0.088$ g/cm³ corresponding to the melting point at a pressure of 1 atm. An annular beam of uranium ions with an energy of 2.7 GeV per nucleon, an inner radius of 0.6 mm and an outer radius of 1.6 mm heats the absorber only which subsequently expands and compresses the hydrogen core inside the cylinder. The number of ions has been varied over two orders of mag-

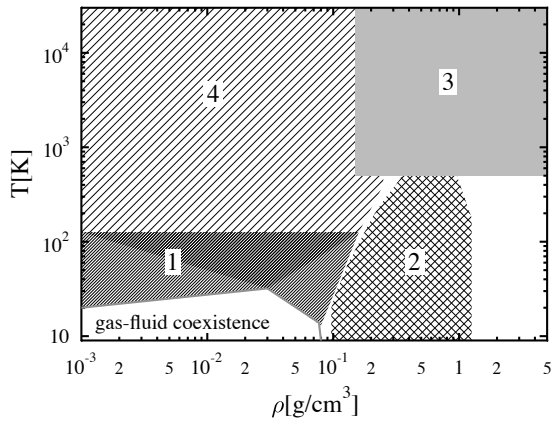


FIG. 1: Density-temperature grid for the hydrogen EOS: NIST and CMC data were used in area 1. The solid hydrogen of region 2 was modeled as described in the text. DFT-MD simulations were used in region 3. The Saumon & Chabrier EOS covers region 4. The gas-fluid coexistence region at low temperatures is indicated. In the white area there is general uncertainty about the EOS.

nitude around 10^{11} particles per bunch with a pulse duration of 20 ns.

The energy deposition of the beam ions in the absorber was modelled using SRIM tables [30]. Since we consider very energetic ions, their stopping range is much longer than the target length which results in a rather uniform heating of the absorber. Accordingly, the hydrodynamic motion will obey a cylindrical symmetry which justifies our use of a 1D code.

The main input quantity for our hydro-simulations is the hydrogen EOS. Since the compression starts from frozen samples, the EOS must cover a wide range of phases including solids, fluids and high temperature/high density plasmas and the well-known transitions between these various phases. Except the SESAME tables [31] such an EOS did not exist. We therefore constructed a new wide range EOS using, for the important regions, largely experimental data or first principle simulation techniques. Uncritical parts are calculated by classical Monte Carlo simulations using potentials fitted to experimental results. In agreement with recent first principles simulations [13, 32], the obtained EOS predicts no plasma phase transition or a phase transition connected to the dissociation of hydrogen molecules in the fluid.

The density-temperature region covered by our EOS is shown in Fig. 1. It spans eight orders of magnitude in the pressure and is free of adjustable parameters. In the different regions, the EOS was determined as follows:

For low temperatures and low densities (region 1), we used experimentally well established data from NIST [33]. These are complemented by classical Monte Carlo simulations using the Ross-Ree-Young intermolecular potential [34, 35]. Both methods agree very well. The NIST data include the gas-solid and gas-liquid phase transition of hydrogen as well as data above the critical point where

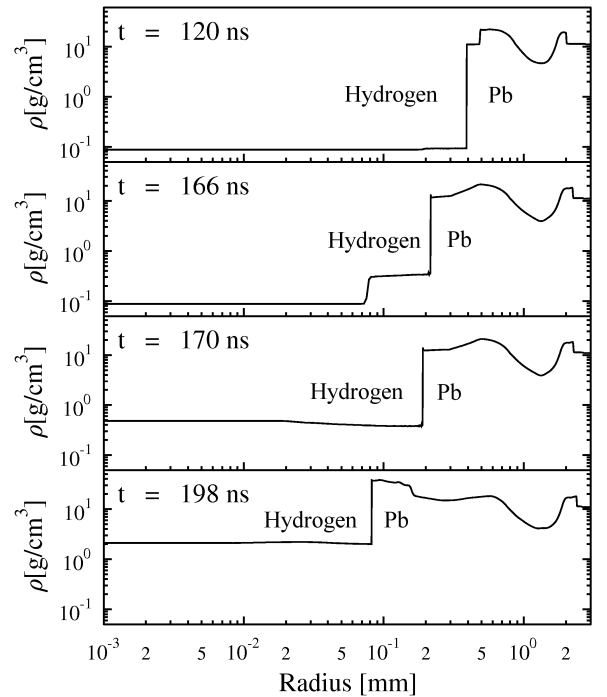


FIG. 2: Density evolution in the target at different stages of compression for lead as the absorber material and a bunch of 10^{12} uranium ions.

molecular hydrogen changes smoothly from gas-like to fluid-like.

For the molecular solid phase of hydrogen (disordered, phase I, region 2), we employed a zero Kelvin isotherm which was determined experimentally up to 40 GPa [36–38]. These data were reproduced and extended to higher pressures by *ab initio* density functional theory (DFT) ground state calculations [39, 40]. Temperature contributions (phonons) were then added by means of a simple Debye model with an experimentally obtained Debye temperature [38].

The high density fluid (region 3) spans molecular and atomic/metallic hydrogen. Here, the EOS was described by means of density functional molecular dynamics simulations (DFT-MD) [13, 41, 42] which allows for a fully quantum-mechanical treatment of the electrons and strong correlations in the ion component.

The EOS of Saumon and Chabrier (S&C) [43, 44] provides data for low density and high temperature systems (region 4). However, DFT-MD calculations were preferred in case the two approaches overlap.

In addition to the hydrogen EOS, we also need data for lead or aluminum to describe the absorber. Compared to the hydrogen, these materials undergo much less dramatic changes. We therefore rely on tabulated EOS data from SESAME [31] for the absorber.

With these EOS data, we now perform the hydrodynamic simulations for ion beam driven compression. Fig. 2 shows a few snapshots of the density evolution in

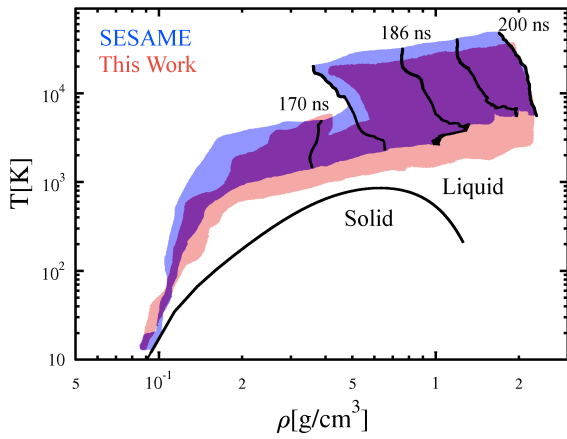


FIG. 3: Trajectories of the hydrogen fluid elements for two EOS models. The lead absorber is heated by bunch of 10^{12} ions. The hydrogen melting line and states that occur simultaneously are marked by black lines.

the target where the time is measured from the beginning of the energy deposition. Since the focal ring of the ion beam is smaller than the absorber, its deposited energy results in the generation of inward and outward propagating shock waves (SW) in the absorber only (see first snapshot at 120 ns). Naturally, the converging SW propagates faster and is stronger than the outgoing SW.

When the converging SW hits the material boundary, a secondary SW is launched into the hydrogen core as it is illustrated in the $t = 166$ ns snapshot. This SW causes the heating of hydrogen due to the entropy jump at the SW front. After hitting the central axis, the SW is reflected and propagates back to the material boundary. At the same time the heated pusher continues to expand and further compresses the hydrogen core. During this relatively slow compression the SW travels back and forth inside the hydrogen slowly increasing its temperature until pressure balance is reached (at $t \approx 200$ ns in the example shown in Fig. 2).

Let us further investigate which states can be tested by ion beam compression. The trajectories of fluid elements in the hydrogen core are marked by the shaded regions in Fig. 3 where the predictions of two EOS models, namely the SESAME tables and our newly constructed EOS, are compared. The regions are bounded by the states in the absorber-hydrogen boundary from below and those located on the axis from above. The trajectories are tracked from the beginning of the compression up to the onset of the expansion of the core. Clearly, the SESAME data predict considerably hotter hydrogen than the new model related to differences in the high temperature/high density region. These differences become much smaller for lower beam intensities (almost negligible for 10^{11} beam ions).

For the high beam intensities used in Fig. 3, the first SW already melts the cryogenic hydrogen which subsequently stays in the molecular fluid region. This region is

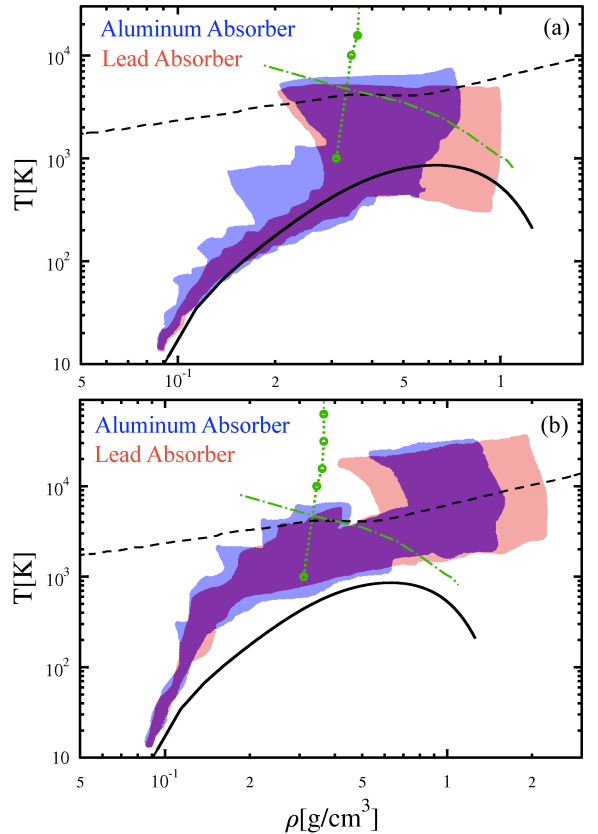


FIG. 4: Temperature-density space reached in hydrogen for two absorbers and two different beam intensities: (a) 10^{11} uranium ions and (b) 10^{12} ions. Shown are the melting line (solid), the isentrope of Jupiter (dashed) [21], states reached by compression with high explosives (dotted) [9], and the transition from molecular to metallic hydrogen (dash-dotted).

of high astrophysical relevance since Jupiter's isentrope [21] runs through the parameter space tested. Moreover, the trajectories of the fluid elements in the hydrogen can be made to closely follow the melting line up to its maximum by carefully choosing lower beam intensities (see Fig. 4). Thus, these are much easier to achieve beam parameters may be preferred if one is interested in probing the phase diagram in the vicinity of the melting line. Since different EOS models predict melting at quite different positions, this gives an excellent opportunity to distinguish between them.

We further investigated different materials as absorber. Fig. 4 shows data for lead and aluminum. Clearly, the heavier lead yields much more homogeneous temperature profiles that can be tuned to test the region of interest and also gives higher compression needed to test the metallic phase. The aluminum EOS is, however, much better understood which gives an advantage for design studies. Again, these differences become more pronounced for higher beam intensities.

It is particularly interesting to notice that the theoretically predicted change in the slope of the melting line

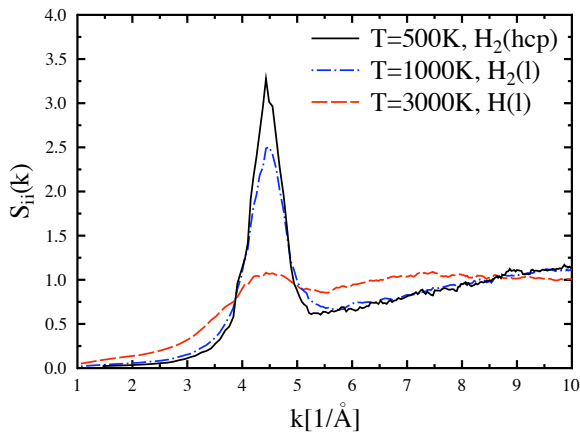


FIG. 5: Structure factors for hydrogen at $P \sim 138$ GPa ($\rho = 0.8$ g/cm³) and different temperatures corresponding to the high pressure molecular solid ($T = 500$ K), molecular liquid ($T = 1000$ K), and metallic liquid ($T = 3000$ K).

[15] is here in reach of an experimental test whereas diamond cell experiments could only reach 50–80 GPa [4, 5]. This is also complementary information to that obtained by states created by explosive compression of hydrogen [9].

The large structural differences of states on different sides of the hydrogen melting line offer an excellent opportunity to be tested by x-ray scattering since the scattering signal is directly proportional to the structure factor [45, 46]. Structure factors obtained by DFT-MD simulations are shown in Fig. 5 for a pressure in the region with negative melting line slope. Most prominent is the peak around 4.5 Å whose height indicates ordering as well as the occurrence of molecules. This makes x-ray scattering very sensitive to the solid-liquid transition as well as to the dissociation of molecules (Mott transition).

The attenuation length of 3 keV x-rays in lead is only around 10 μ m which makes probing through the lead impossible. However, forward scattering through the ends of the cylinder can avoid the lead. The shift of the Compton line and the plasmon are sensitive to the density under these conditions while the width of the Compton line indicates the electron temperature. The height of the elastic scattering peak finally gives the structural information wanted.

Financial support from the EPSRC (UK) is gratefully acknowledged. The work of SHG was performed under the auspices of the U.S. Department of Energy by Lawrence Livermore National Laboratory under Contract DE-AC52-07NA27344.

-
- [1] H. Mao, R. J. Hemley, *Rev. Mod. Phys.* **66**, 671, (1994).
 [2] R. J. Hemley *et al.*, *Phys. Rev. Lett.* **76**, 1667 (1996).
 [3] P. Loubeyre, F. Occelli, and R. LeToullec, *Nature* **416**,

- 613 (2002).
 [4] E. Gregoryanz *et al.*, *Phys. Rev. Lett.* **90**, 175701 (2003).
 [5] S. Deemyad and I. F. Silvera, *Phys. Rev. Lett.* **100**, 155701 (2008).
 [6] S. T. Weir, A. C. Mitchell, and W. J. Nellis, *Phys. Rev. Lett.* **76**, 1860 (1996).
 [7] G. W. Collins *et al.* *Phys. Rev. Lett.* **87**, 165504 (2001).
 [8] M. D. Knudson *et al.* *Phys. Rev. Lett.* **90**, 035505 (2003).
 [9] V. E. Fortov *et al.*, *Phys. Rev. Lett.* **99**, 185001 (2007).
 [10] G. E. Norman and A. N. Starostin, *High Temp.* **6**, 394 (1968).
 [11] D. Beule, *et al.*, *Phys. Rev. B* **59**, 14177 (1999).
 [12] S. Scandolo, *Proc. Nat. Acad. Sci. USA* **100**, 3051 (2003).
 [13] J. Vorberger *et al.*, *Phys. Rev. B* **75**, 024206 (2007).
 [14] B. Jakob *et al.*, *Phys. Rev. E* **76**, 036406 (2007).
 [15] S. A. Bonev *et al.*, *Nature* **431**, 669 (2004).
 [16] E. Babaev, A. Sudbe, and N. W. Ashcroft, *Nature* **431**, 666 (2004).
 [17] M. Mayor and D. Queloz, *Nature* **378**, 355 (1995).
 [18] A. Burrows, *Nature* **433**, 261 (2005).
 [19] The extrasolar planet encyclopedia. <http://exoplanet.eu>.
 [20] T. Guillot *et al.*, in *Jupiter*, F. Bagenal, Ed. (Univ. of Arizona Press, Tucson, 2003), chap. 3, pp. 35-57.
 [21] B. Militzer *et al.*, submitted to *ApJL*.
 [22] J. D. Lindl, *Inertial Confinement Fusion* (Springer-Verlag, New York, 1998).
 [23] S. Atzeni and J. Meyer-ter-Vehn, *The Physics of Inertial Fusion* (Clarendon Press, Oxford, 2004).
 [24] M. Tabak *et al.*, *Phys. Plasma* **12**, 057305 (2005).
 [25] N. A. Tahir *et al.*, *Phys. Rev. E* **63**, 016402 (2000).
 [26] N. A. Tahir *et al.*, *Phys. Rev. Lett.* **95**, 035001 (2005).
 [27] N. A. Tahir *et al.*, *Phys. Rev. B* **67**, 184101 (2003).
 [28] A. A. Samarskii and Y. P. Popov, *Difference Methods for the Solution of Problems of Gas Dynamics*, (*Nauka, Moscow, 1980*) (in Russian).
 [29] B. van Leer, *J. Comput. Phys.* **135**, 299 (1997).
 [30] J. Ziegler, SRIM 2006.2. <http://www.srim.org>.
 [31] G. I. Kerley, Los Alamos Scientific Laboratory Report No. LA-4776, UC-34. http://t1web.lanl.gov/newweb_dir/t1sesamereginfo.html.
 [32] J. Vorberger *et al.*, *Contrib. Plasma Phys.* **47**, 375 (2007).
 [33] E. W. Lemmon, M. O. McLinden, and D. G. Friend, in *NIST Standard Reference Database 69*, P. J. Linstrom and W. G. Mallard, Eds. (Nat. Inst. Standards and Technology, Gaithersburg, 2005).
 [34] B. Militzer, *Coulomb Monte Carlo (CMC)*.
 [35] M. Ross, F. H. Ree, and D. A. Young, *J. Chem. Phys.* **79**, 1487 (1983).
 [36] J. K. Krause and C. A. Swenson, *Phys. Rev. B* **21**, 2533 (1980).
 [37] V. Diatschenko *et al.*, *Phys. Rev. B* **32**, 381 (1985).
 [38] R. J. Hemley *et al.*, *Phys. Rev. B* **42**, 6458 (1990).
 [39] M. Fuchs and M. Scheffler, *Comp. Phys. Com.* **119**, 67 (1999).
 [40] Copyright ABINIT group (M. Mikami, J. M. Beuken, X. Gonze) 2003-2005.
 [41] I. Tamblyn and S. A. Bonev, to be published
 [42] J. Vorberger and B. Militzer, to be published
 [43] D. Saumon and G. Chabrier, *Phys. Rev. A* **46**, 2084 (1992).
 [44] D. Saumon, G. Chabrier, and H. M. Van Horn, *Astrophys. J. Suppl.* **99**, 713 (1995).
 [45] S. H. Glenzer *et al.*, *Phys. Rev. Lett.* **90**, 175002 (2003).
 [46] S. H. Glenzer *et al.*, *Phys. Rev. Lett.* **98**, 065002 (2007).